Mapping Protein−Protein Interactions within a Stable Complex of DNA Primase and DnaB Helicase from *Bacillus stearothermophilus*†

Louise E. Bird,‡ Hu Pan,‡ Panos Soultanas,‡ and Dale B. Wigley*

Sir William Dunn School of Pathology, University of Oxford, South Parks Road, Oxford OX1 3RE, U.K.

Received August 11, 1999; Revised Manuscript Received October 26, 1999

ABSTRACT: For the first time, we demonstrate directly a stable complex between a bacterial DnaG (primase) and DnaB (helicase). Utilizing fragments of both proteins, we are able to dissect interactions within this complex and provide direct evidence that it is the C-terminal domain of primase that interacts with DnaB. Furthermore, this C-terminal domain is sufficient to induce maximal stimulation of the helicase and ATPase activities of DnaB. However, the region of DnaB that interacts with the C-terminal domain of primase appears to comprise a surface on DnaB that includes regions from both of the previously identified N- and C-terminal domains. Using a combination of biochemical and physical techniques, we show that the helicase−primase complex comprises one DnaB hexamer and either two or three molecules of DnaG. Our results show that in *Bacillus stearothermophilus* the helicase−primase interaction at the replication fork may not be transient, as was shown to be the case in *Escherichia coli*. Instead, primase appears to interact with the helicase forming a tighter complex with enhanced ATPase and helicase activities.

The replication of DNA in bacteria and bacteriophages requires a number of enzymes, including replicative helicase and primase activities. The most widely studied bacterial replication system is that of *Escherichia coli*, in which the replicative helicase is DnaB and the primase is DnaG (*1*). Primase plays a key role on the lagging strand during DNA replication. It has been proposed that primase, DnaB, and the DNA polymerase III holoenzyme (Pol III HE)[1] form a dynamic protein complex at the replication fork so that the functions of all three enzymes are coordinated collectively (*1*, *2*). The Pol III HE has been shown to interact with primase in a replication fork system reconstituted in vitro, and this interaction limits the size of the nascent primers to the size of the physiological range of 9−14 nucleotides (*3*). The *E. coli*, DnaB protein associates transiently with the primase (*4*) and introduces the primase to the replication fork, thus activating its priming activity. Consequently, the interaction of primase with the replication fork is distributive. In fact, the cyclic association of primase with the replication fork, with a consequent commitment to priming, is a key event during lagging-strand synthesis, forcing both the initiation of a new cycle of Okazaki fragment synthesis and the termination of synthesis of the preceding Okazaki fragment by the lagging-strand polymerase (*5*). However, in other systems, such as the gene 4 proteins of bacteriophage T7, the two activities are contained within a single multifunctional protein and are, therefore, in a permanent association with each other (*6*).

The replicative helicase, DnaB, uses the energy of ATP hydrolysis to unwind the duplex DNA at a replication fork (*7*). It is a hexameric protein comprising 52 kDa subunits (*8*, *9*). In addition to acting as a helicase, DnaB may be regarded as being a multifunctional enzyme since it interacts with a number of other proteins during replication of DNA. Interactions include those with DnaA, DnaC, DnaG, and the τ subunit of DNA polymerase III (*2*, *4*, *10*−*12*). These interactions function to initiate replication of DNA (*10*), to increase the rate of movement of the replication fork (*12*), and to assemble part of the primosome (*13*). The interaction of DnaB with DnaG in the primosome regulates the synthesis of oligoribonucleotides used to prime DNA synthesis on the lagging strand (*2*, *4*).

In the Gram-positive bacterium *Bacillus subtilis*, the primosome is less well understood and the replicative helicase and primase enzymes were identified by their similarity to their *E. coli* counterparts (42 and 30% identity, respectively; *14*, *15*). However, it has been suggested that the other components of the *B. subtilis* primosome (with the exception of PriA) are different from those of *E. coli* (*16*). This raises the possibility that the *B. subtilis* primosome may be structurally different from its *E. coli* counterpart. A structural difference between the *B. subtilis* and *E. coli* primosomes may also reflect functional diversity and may imply that the primosomes in these two organisms employ different biochemical mechanisms. In an effort to study the biochemical mechanism of DNA replication enzymes in *Bacillus* and compare it to that of *E. coli*, we have cloned the replicative helicase (dnaB) (*17*) and primase (dnaG) (*18*)

† This work was supported by Wellcome Trust Grant 046666 and a Medical Research Council studentship to H.P. (G78/4931).

* To whom correspondence should be addressed. Phone: + 44 1865 285479. Fax: + 44 1865 275515. E-mail: wigley@eric.path.ox.ac.uk.

‡ These authors contributed equally to this work and should therefore be considered as joint first authors.

[1] Abbreviations: Pol III HE, DNA polymerase III holoenzyme; nt, nucleotides; NEB, New England Biolabs; SDS−PAGE, sodium dodecyl sulfate−polyacrylamide gel electrophoresis; LB, Luria-Bertani; PMSF, phenylmethanesulfonyl fluoride; PCR, polymerase chain reaction; DTT, dithiothreitol; EDTA, ethylenediaminetetraacetic acid; TBE, tris-borate-ethylenediaminetetraacetic acid; ssDNA, single-stranded deoxyribonucleic acid; NMR, nuclear magnetic resonance; ADPNP, adenylyl imidodiphosphate.

10.1021/bi9918801 CCC: $19.00
Published on Web 12/09/1999

genes from *Bacillus stearothermophilus* NCA 1503, determined their nucleotide sequences, and expressed both proteins in *E. coli*. To remain consistent with the *E. coli* nomenclature, we have designated the *B. stearothermophilus* replicative helicase as DnaB and the primase as DnaG. In this work, we have used fragments of DnaB and DnaG to investigate their domain structures and characterize the distinct biochemical functions associated with discrete physical domains, as a prelude to structural studies. We also demonstrate that, unlike *E. coli* DnaB and DnaG, the *B. stearothermophilus* proteins form a stable complex that can be isolated by gel filtration. Finally, we characterize this complex biochemically and analyze the contributions made by different domains of both proteins to its formation and biochemical activities.

EXPERIMENTAL PROCEDURES

Materials, Enzymes, Nucleotides, and Vectors. All restriction and modification enzymes were purchased from New England Biolabs (NEB), Boehringer Mannheim, or Gibco-BRL and used according to the manufacturer's instructions. *E. coli* DnaB was a gift from K. Marians. All columns and column resins were purchased from Pharmacia. Radiolabeled nucleotides were purchased from Amersham. pSP73 and pET21d, and pET22d, plasmids were purchased from Promega and Novagen, respectively. pUC19 and M13mp18/19 were purchased from NEB. Oligonucleotides were synthesized using an Applied Biosystems model 381A DNA synthesizer, deprotected by incubation at 65 °C for 4 h, and purified using G200 NAP10 columns (Pharmacia) according to the manufacturer's instructions. Plasmid DNA was made using Qiaspin columns (Qiagen) according to the manufacturer's protocols. Cloning, overexpression, and purification of DnaB and DnaG proteins were reported elsewhere (*17*, *18*). These references also give details about the construction of pGDNAB and pDNAB (carrying the dnaB gene) and pUC19-BSpri and pET21d-pri (carrying the dnaG gene) plasmids. During the last purification step (gel filtration), the absorbance at 260 and 280 nm was monitored to ensure that no nucleic acid contaminant was present in the purified protein preparations. Concentration values for all proteins described in the text refer to monomers, while concentration values for DNA refer to molecules, unless otherwise stated.

Strains and Cloning Vectors. The following strains of *E. coli* were used as hosts for pUC19-, pET21d-, and pET22d-based constructs. MC1061 *F*$^-$, *araD139, D (ara-leu)7696, galH, E15, galK16, D (lac)X74, rpsL, (Str*^{R}*), hsdR2 (*$r_K{}^{--}$, $m_K{}^+$*), mcrA, mcr* B1 (*19*) and XL1-Blue *supE44, hsdR17, recA1, endA1, gyrA96, thi, relA1, [F′ proAB*$^+$*, lacIqZDM15:: Tn10 (tet*^{R}*)]* (*20*) were used for cloning, and B834(DE3) *F*$^-$, *ompT, hsdS*$_B$*, (*$r_B{}^-$, $m_B{}^{--}$*), gal, met, dcm* (*21*) was used for protein production. *E. coli* strains were grown aerobically in LB (or on LB plates) containing 100 μg/mL ampicillin.

General Methods. DNA transformations and manipulations were performed essentially as described previously (*22*). N-Terminal sequencing of the proteolytic fragments was carried out using an Applied Biosystems model 470A protein sequenator connected to an on-line 120A high-pressure liquid chromatograph. SDS−PAGE analysis was carried out as described previously (*23*). Gels were stained with Coomassie Brilliant Blue and destained in 10% acetic acid and 25% methanol.

Limited Proteolysis of Primase. Limited proteolysis of purified DnaG was carried out with proteases endoproteinase Glu-C from *Staphylococcus aureus* strain V8 and trypsin. The protein was digested with protease at different protein-to-protease ratios at room temperature for 30 min in buffer containing 50 mM Tris (pH 7.5), 50 mM KCl, 5 mM $MgCl_2$, and 10% glycerol. The reactions were terminated by addition of PMSF to a final concentration of 2 mM, and SDS−PAGE loading buffer, followed by heating to 95 °C for 5 min. The samples were then loaded immediately onto a 15% SDS−polyacrylamide gel for analysis.

Construction of Vectors for Expressing the Truncated Fragments of Primase (P49, P37, P16, and P12). Proteolytic fragments of DnaG were produced from the intact protein using trypsin proteolysis. N-Terminal sequencing and DNA sequencing were subsequently used to precisely locate the proteolytic sites in the dnaG gene. On the basis of these studies, we identified the coding sequences for P49, P37, P16, and P12. PCR was then used to amplify and clone these coding sequences in the pET21d expression vector as described below. All constructs were sequenced to verify the absence of spurious mutations that might have been introduced during the PCRs.

P37. The coding region of P37 was amplified by PCR using pUC19-BSpri as a template and the following primers: 5′-primer, 5′-GATATA**CC ATG G** GG CGC GAT GGT CAG-3′; and 3′-primer, 5′-GCATCC **AAGC TT**A CCT CTC CGC CTG GCT GCG-3′. The 5′-primer contained a *Nco*I site (shown in bold) and an initiator codon introduced just upstream from amino acid 106. The 3′-primer contained a stop codon introduced downstream from amino acid 466 and a *Hin*dIII site (shown in bold) after the stop codon. The PCR product of the P37 coding sequence was cloned into pUC19 to give pUC19-p37(PCR). A *Sph*I−*Cla*I fragment from pUC19-BSpri (carrying the original dnaG gene) was used to replace the equivalent *Sph*I−*Cla*I fragment of pUC19-p37(PCR). The pUC19-p37 plasmid was subsequently digested with *Nco*I and *Hin*dIII, and the resulting fragment carrying the P37 coding sequence was cloned into pET21d to give the pET21d-p37 expression vector.

P49. The pET21d-p49 expression vector carrying the coding sequence of P49 was constructed by isolating the *Cla*I−*Hin*dIII fragment from pET21d-p37 and introducing it into the *Cla*I−*Hin*dIII-digested pET21d-BSpri plasmid to give the final pET21d-p49 expression vector.

P16. The P16 coding region was amplified by PCR using the pUC19-BSpri plasmid as a template and the following primers: 5′-primer, 5′-GATATA**CC ATG G** CG AAA AAG TTG CTG CCG-3′; and 3′-primer, 5′-GCATCC **AAGC TT**A AAC ATC CAG CTC ATA GAC GGA-3′. The 5′-primer contained a *Nco*I site (shown in bold) and an initiator codon at amino acid 451. The 3′-primer contained the stop codon after the last residue of primase and a *Hin*dIII site (shown in bold). The PCR product containing the P16 coding sequence was digested with *Nco*I−*Hin*dIII and cloned into the equivalent sites in pUC19 to give the pUC19-p16(PCR) plasmid. The *Nde*I−*Hin*dIII fragment from the pUC19-BSpri plasmid was then used to replace the equivalent fragment in pUC19-p16(PCR). The pUC19-p16(PCR) plasmid was then digested with *Nco*I−*Hin*dIII, and the resulting fragment containing the coding sequence for P16 was cloned into pET21d to give the final pET21d-p16 expression vector.

P12. The coding region of P12 was amplified by PCR using the pUC19-BSpri as a template and the following primers: 5′-primer, 5′-GATATA**CCATGG**GACATCG-CATTCCCG-3′; and 3′-primer, 5′-GCATCC**AAGCTT**AAA-CATCCAGCTCATAGACGGA-3′. The 5′-primer contained a *Nco*I site (shown in bold) and a start codon. The 3′-primer contained a stop codon introduced downstream from amino acid 104 and a *Hin*dIII site (shown in bold) after the stop codon. The PCR product was cloned into pUC19 to give pUC19-p12e(PCR). Finally, the *Nco*I−*Hin*dIII fragment from pUC19-p12e(PCR) was isolated and cloned into pET21d to give the final expression vector pET21d-p12e.

Overexpression and Purification of the Truncated Primase Fragments (P49, P37, P16, and P12). P49. Overexpression and purification of P49 were carried out as described previously for the intact primase (*18*). The fractions containing protein that eluted from the Hi-Trap Heparin column were pooled and diluted in buffer C [50 mM Tris (pH 8.5), 2 mM EDTA, and 1 mM DTT] to reduce the conductivity to less than 10 mS. The protein was then loaded onto a Source Q column pre-equilibrated with buffer C. The column was washed with buffer A [50 mM Tris (pH 7.5), 2 mM EDTA, and 1 mM DTT], and the protein was eluted with a gradient of 0 to 400 mM NaCl in buffer C. Trace contaminants were removed by gel filtration on a Superdex S75 column in buffer A and 200 mM NaCl.

P16. Overexpression and purification of P16 were carried out as decribed previously for the intact primase. The final step of purification was gel filtration on a Superdex S75 column in buffer A and 200 mM NaCl.

P12. Overexpression and purification of P12 were as described for the intact primase. After ammonium sulfate precipitation, the pellet was resuspended in buffer A to a volume such that the conductivity was less than 10 mS. The protein was then applied onto a Source Q column pre-equilibrated with buffer A, and after being washed in buffer A, it was eluted with a 0 to 300 mM NaCl gradient in buffer A. Trace contaminants were removed by gel filtration on a Superdex S75 column in buffer A and 200 mM NaCl. Alternatively, P12 can also be purified by proteolysis of the intact primase as described below for P37.

P37. The pET21d-p37 expression vector failed to overexpress P37, and P37 was eventually purified using trypsin digestion of full-length primase. The purified primase was concentrated using a Centricon 50 concentrator (Amicon) to 5 mg/mL and exchanged into proteolysis buffer. The reaction was started by adding trypsin at a trypsin-to-primase molar ratio of 1:200 and carried out at room temperature for 30 min. The reaction was terminated by addition of PMSF to a concentration of 2 mM. The digestion products were separated by gel filtration on a Superdex S75 column in buffer A and 200 mM NaCl. The purity of all proteins was monitored on SDS−polyacrylamide gels and was greater than 99% in all cases.

Determination of the Zinc Content of Intact Primase and Its Truncated Fragments. The zinc content of primase and its proteolytic fragments was measured by flame atomic absorption spectroscopy. Protein samples were prepared in ultrapure water with 50 mM Tris (pH 7.5), 200 mM NaCl, 2 mM DTT, and 10% glycerol. The standard solution of zinc was prepared with 1 ppm zinc in the same solution as the proteins.

Cloning and Overexpression of the P17 and P33 Fragments of DnaB. The coding regions for P17 and P33 were amplified by PCR using pGDNAB as a template. The 5′- and 3′-primers used to synthesize the full-length gene (*18*) together with primers BSTBP17R (5′-GCATCTAAGCT-TACTTCCGTTGGGAAACCTCCATAAT-3′) and BSTBP-33F (5′-GCATATATCATATGCATTCGGGCGCCTTTAA-AAAT-3′) were used for P17 and P33, respectively. The *Nde*I−*Hin*dIII-restricted PCR products were cloned into *Nde*I−*Hin*dIII-cut pET22d, and the resulting expression vectors were designated pET22-p17 and pET22-p33.

Purification of Truncated DnaB Fragments. P17. Overexpression of P17 was as described for the intact DnaB except for the resuspension of the harvested cells which was carried out in buffer A and 10% sucrose. The clarified cellular lysate was applied to a 20 mL Source Q column. The protein was eluted with a 200 mL gradient of 0 to 400 mM NaCl in buffer A. Trace contaminants were removed by gel filtration in a Superdex S75 column in buffer A and 100 mM NaCl.

P33. Overexpression and the initial stage of purification were as described for P17. The peak fractions from the Source Q column were pooled and diluted with water until the conductivity was equal to that of buffer A and 25 mM NaCl. The pool was applied to a 5 mL Hi-Trap Heparin column pre-equilibrated with buffer A. The column was washed with 2 column volumes of buffer A, and the protein was eluted with a 75 mL gradient of 0 to 2 M NaCl in buffer A. Trace contaminants were removed by gel filtration in a Superdex S200 column in buffer A and 100 mM NaCl.

ATPase Assays. ATP hydrolysis was monitored using a coupled assay by linking it to NADH oxidation (*24*). The reaction mixtures (1 mL) contained 20 mM Tris (pH 7.5), 50 mM NaCl, 0.1 mM EDTA, 10 mM $MgCl_2$, 5 mM DTT, enzyme (24 and 27 nM for intact DnaB and P33, respectively), and ATP in the presence or absence of a 50-fold molar excess of a single-stranded 81mer oligonucleotide (*25*). Reactions were initiated by addition of DnaB, and the rate of ATP hydrolysis was monitored by following NADH oxidation at 340 nm. The ATP used in these studies was purchased from Sigma (catalog no. A 5394) and was 99−100% pure. Although ATPase activity is expressed as molecules of ATP hydrolyzed per second per protein monomer, it is unlikely that all the monomers of the hexameric ring (or a dimeric P33 complex) will be hydrolyzing ATP at the same rate (see Results and Discussion).

Helicase Assays. The DNA substrate for the helicase reactions was prepared by labeling a 68mer oligonucleotide at the 5′-end using T4 polynucleotide kinase and annealing it to ssM13mp18 DNA (*25*). The unannealed oligonucleotide and free label were removed by centrifugation through a S400 micro-spin column (Pharmacia). The annealed oligonucleotide produced a substrate with both 5′- and 3′-tails. Unless otherwise stated, helicase reaction mixtures contained 20 mM Tris (pH 7.5), 50 mM NaCl, 10 mM $MgCl_2$, 5 mM DTT, 10% glycerol, 1 nM DNA substrate, 100 nM enzyme (referring to monomer), and 3 mM ATP. Reactions were initiated by addition of ATP at 37 °C and terminated after 30 min by adding 0.2 volume of 2% SDS, 200 mM EDTA, and 50% glycerol. Reactions carried out at 50 °C did not reveal any significant difference in helicase activity (data not shown). Electrophoresis was carried out with 10%

nondenaturing gels containing TBE (*22*). After electrophoresis, gels were dried under vacuum and autoradiographed at −80 °C with Fuji RX X-ray film.

Analytical Gel Filtration. Protein samples were concentrated using a Centricon 30 concentrator (Amicon), and gel filtration was performed at room temperature using either a Superdex 200 HR 10/30 column or a Superdex 75 HR 10/30 column. The columns were equilibrated with 50 mM Tris (pH 7.5), 1 mM EDTA, 1 mM DTT, and 100 mM NaCl, unless stated otherwise. The apparent molecular mass (M_{app}) was calculated from an interpolation of a semilog plot of the partition coefficient (K_{av}) of the protein markers [thyroglobulin (669 kDa), β-galactosidase (464 kDa), myosin (410 kDa), bovine serum albumin dimer (132 kDa), phosphorylase *b* (97 kDa), bovine serum albumin monomer (66 kDa), and ovalbumin (45 kDa)] versus molecular masses (data not shown).

Analytical Ultracentrifugation. Sedimentation equilibrium measurements were carried out in the Optima XL-A ultracentrifuge (Beckman) using the An-60Ti analytical rotor. All runs were performed at various protein concentrations, at 20 °C, at the appropriate speed. The data were fitted to the equation for a single ideal species and analyzed using the Microcal Origin program. Residual data were also analyzed to ensure that there was no deviation from ideality.

The equation for a single ideal species is $C_r = C_F e^{(\omega^2/2RT)M(1 - \upsilon\rho)(r^2 - F^2)}$, where C_r is the solute concentration at radius r, C_F is the solute concentration at a reference distance F (the choise of F is arbitrary), ω is the angular velocity ($\omega = 2\Pi/60$ rpm), R is the gas constant (8.314×10^7 erg mol^{-1} K^{-1}), T is the temperature in kelvin, M is the gram molecular mass of the particle, V is the partial specific volume of the particle, and ρ is the density of the solvent.

Analysis of the data results in estimates of the buoyant molecular mass at equilibrium [buoyant molecular mass = $M(1 - \upsilon\rho)$], from which M can be derived.

RESULTS AND DISCUSSION

Proteolytic Digestion of B. stearothermophilus Primase. Digestion of primase with trypsin at room temperature at different primase-to-trypsin ratios resulted in the progressive degradation of the full-length 67 kDa polypeptide (Figure 1A). The first two polypeptide fragments to appear had apparent molecular masses of 49 (P49) and 16 kDa (P16). As the digestion progressed, a 37 kDa (P37) fragment and a 12 kDa (P12) fragment also appeared.

The locations of the trypsin digestion sites were identified by determining the N-terminal amino acid sequence of the resulting fragments (Table 1 and Figure 1B). The N-terminal amino acid sequence of P49 was identical to that of the intact primase, indicating that this fragment, accounting for more than two-thirds of the polypeptide chain, is the N-terminal fragment. The amino acid sequence of the C-terminal P16 fragment was KLLPAFQN, suggesting that the first tryptic cut occurred between amino acids 454 (K) and 455 (K), thus generating P49 and P16. The N-terminal amino acid sequence of P37 was GRDDGQTD. P37 was identified as the C-terminal fragment resulting from the cleavage of P49, the other product being the P12 N-terminal fragment which contains a zinc-binding motif. The P37, P16, and P12 fragments were markedly resistant to further digestion by trypsin. Limited proteolysis of the primase with protease V8 produced similar fragments (data not shown). P49 contains all of the primase and the zinc-binding motifs and is likely to encompass the primer synthesis domain. P37 contains all of the primase motifs except the zinc-binding motif, the latter residing in the P12 fragment.

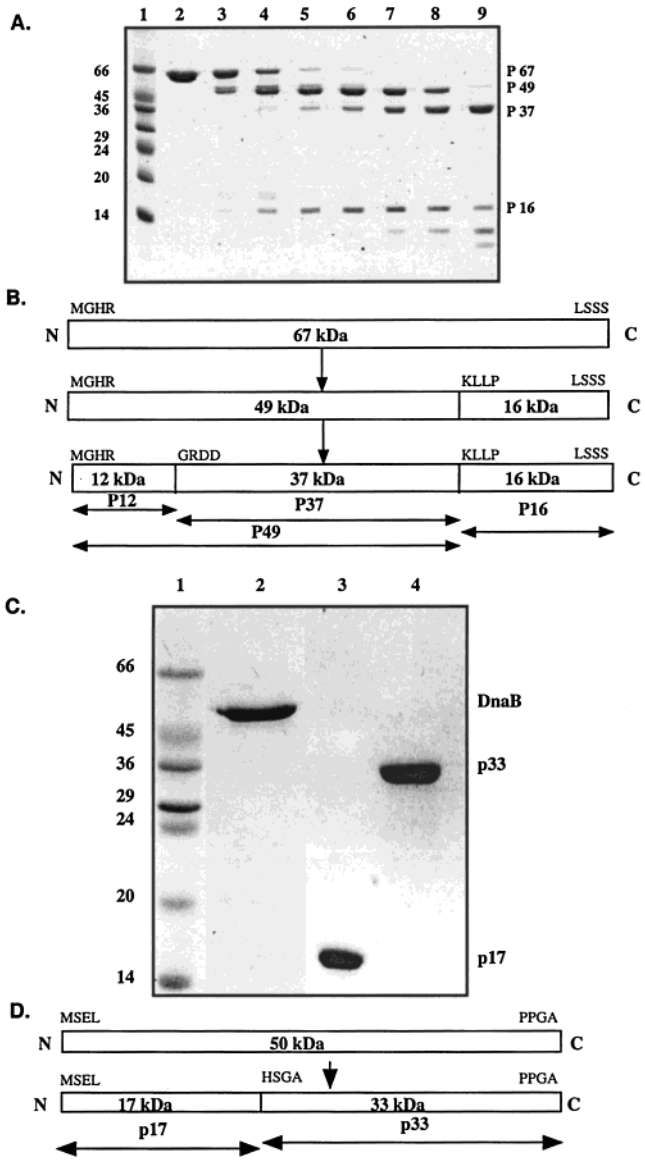

FIGURE 1: (A) SDS−PAGE analysis of the *B. stearothermophilus* DnaG fragments produced by trypsinolysis. DnaG (25 μg) was digested with increasing amounts of trypsin from lane 1 to 8 (0, 1, 2.5, 5, 10, 25, 50, and 100 ng). (B) Schematic representation of the DnaG fragments produced by proteolysis. (C) SDS−PAGE analysis showing the full-length and the two purified fragments of *B. stearothermophilus* DnaB. (D) Schematic representation of the DnaB fragments produced by proteolysis. The digestion sites for both proteins are indicated in the schematic diagrams.

Table 1: Fragments of *B. stearothermophilus* DnaB and DnaG Proteins

protein	fragment	N- and C-termini
DnaB	P33	^{155}HSGA.....PPGA^{454}
	P17	^{1}MSEL.....SQRK^{154}
DnaG	P49	^{1}MGHR.....MLAK^{454}
	P37	^{106}GRDD.....MLAK^{454}
	P16	^{455}KLLP.....LSSS^{597}
	P12	^{1}MGHR.....LDVR^{105}

Table 2: Zinc Content of *B. stearothermophilus* Primase and Its Domain Proteins

protein	$[Zn^{2+}]$ (μM)	[protein] (μM)	zinc (g-atom/mol)
primase	23.3	35.8	0.65
primase−Zn^{2+}	12.2	18.9	0.65
P49	14.3	25.5	0.56
P49−Zn^{2+}	15.0	24.9	0.60
P12	8.7	15.6	0.56
P37	0.07	28.2	0.002

Expression vectors for all the truncated fragments of DnaG were constructed by cloning their coding sequences into pET21d. All truncated fragments (with the exception of P37) were overexpressed and subsequently purifed. P37 was not overexpressed and was therefore purified by tryptic digestion of the intact full-length DnaG. P37 was the major product of trypsinolysis and could easily be separated from the other products by gel filtration. P12 was a byproduct of this procedure and could also be purified by gel filtration. The proteins produced by this method were greater than 99% pure, and typically, 1 mg of intact DnaG yielded 0.5 mg of P37 and 0.2 mg of P12.

Although all DNA primases have a potential zinc-binding site in the N-terminal region of the protein, only two other primases, *E. coli* primase and T7 gene 4 primase, have been shown directly to be zinc metalloproteins (*26*, *27*). We determined the zinc content of *B. stearothermophilus* primase and its proteolytic fragments by atomic absorption spectroscopy (Table 2). We found that there is a significant amount of zinc in DnaG, P49, and P12, but not in P37. This is not unexpected, because P37 is formed from P49 by a deletion of the proposed zinc-binding domain, P12. To investigate whether primase or P49 chelates additional zinc from the environment during protein expression, we added 1 mM zinc acetate to the growth medium during overexpression and measured the zinc content in each of the purified proteins. The zinc contents of primase and P49 were the same as when zinc acetate was not included in the growth medium. As expected, our data show that it is the N-terminal 12 kDa of *B. stearothermophilus* primase that contains the bound zinc ion. We have recently determined the crystal structure of the P12 fragment, and the presence of the zinc ion is confirmed in this structure (unpublished data).

The first primase to be identified and characterized was that from *E. coli*. Most of the information concerning the functional domains of primase, protein−protein interactions, and enzymatic mechanisms of replication was based on the development of priming systems involving primer synthesis by *E. coli* primase in vitro. *E. coli* primase comprises two functional domains, an N-terminal 49 kDa domain that retains primase activity in replication assays and a C-terminal 16 kDa domain that is required for functional interaction with DnaB (*28*). Our data on *B. stearothermophilus* primase are consistent with the results reported for *E. coli* primase (*2*). We also confirm that P49 comprises two distinct structural domains, P37 (containing all of the primase domains) and P12 (containing the zinc-binding domain) which are resistant to further tryptic digestion and can be separated by gel filtration.

B. stearothermophilus DnaB Forms a Stable Hexamer. E. coli DnaB was reported to be hexameric under a wide variety of conditions (*8*, *9*). The hexamer was observed to be in a dynamic equilbrium with lower-order oligomers, in particular a trimer. Formation of a hexamer is necessary for the activity of all hexameric helicases (*29*). Here we compare the oligomeric state of *B. stearothermophilus* DnaB with that of *E. coli* DnaB using analytical gel filtration. *E. coli* DnaB eluted as a hexamer at high concentrations and as lower-order oligomers at low concentrations (Figure 2A), confirming previous observations of a dynamic equilibrium between various oligomeric states. In contrast, *B. stearothermophilus* primase eluted as a hexamer over all concentrations that were tested with a higher-molecular mass shoulder, suggesting that a small amount of a higher-order oligomer was also present (Figure 2B). Separation of the hexamer from this higher-order oligomer, followed by another gel filtration, eliminated this shoulder, revealing that the hexamer is not in equilibrium with the higher-order oligomer (data not shown). Analytical ultracentrifugation experiments at 1 μM DnaB also confirms the existence of a stable hexamer, with a molecular mass of 295 kDa (Figure 2C). Thus, under these conditions, the *B. stearothermophilus* DnaB hexamer is much more stable than the *E. coli* enzyme.

Structural Characterization of DnaB. Previous studies with *E.coli* DnaB using limited trypsinolysis revealed that the protein could be cleaved into two fragments representing two major domains (*30*, *31*). On the basis of these data and using amino acid sequence comparisons, we identified the equivalent trypsinolysis site in the *B. stearothermophilus* DnaB at residue 172 (*18*). Cleavage at this site will give rise to the amino- (P17) and carboxy-terminal (P33) domains of 17 and 33 kDa, respectively (Figure 1D). Using PCR, we amplified and cloned the coding sequences of these fragments into the pET22d vector to produce overexpressing vectors. Both truncated DnaB fragments were overexpressed in *E. coli* and purified successfully (Figure 1C).

The C-terminal domain (P33) retained the motifs associated with the helicase activity and formed stable dimers and unstable hexamers. At high salt levels and at high protein concentrations, P33 eluted with a predicted molecular mass of 160 kDa (Figure 3A), close to that expected for a hexamer (197 kDa). Lower-order oligomers were also observed, suggesting that the P33 hexamers were less stable than the full-length DnaB. As the protein concentration was decreased, the apparent molecular mass of the peak also decreased. Thus, the interactions between P33 monomers are weaker than those of the full-length protein, and the P33 hexamer therefore exists in a dynamic equilibrium with lower-order oligomers, suggesting that although the N-terminal region of the protein contributes to the stability of the hexamer it is not required for hexamerization per se. Interestingly, at 500 mM NaCl, P33 formed stable hexamers (Figure 3B). The formation of stable hexamers under these conditions supports previous observations from our laboratory which show that the C-terminal domains of hexameric helicases possess all of the attributes necessary for helicase activity (*32*, *33*).

The oligomeric state of P17 was also analyzed by gel filtration over a range of protein concentrations (Figure 3C). Its apparent molecular mass decreased with decreasing protein concentration, suggesting that the *B. stearothermophilus* P17 truncated protein is in a dynamic monomer−dimer equilibrium in solution, in contrast to the *E. coli* P17 protein which was shown to be monomeric in solution (*30*).

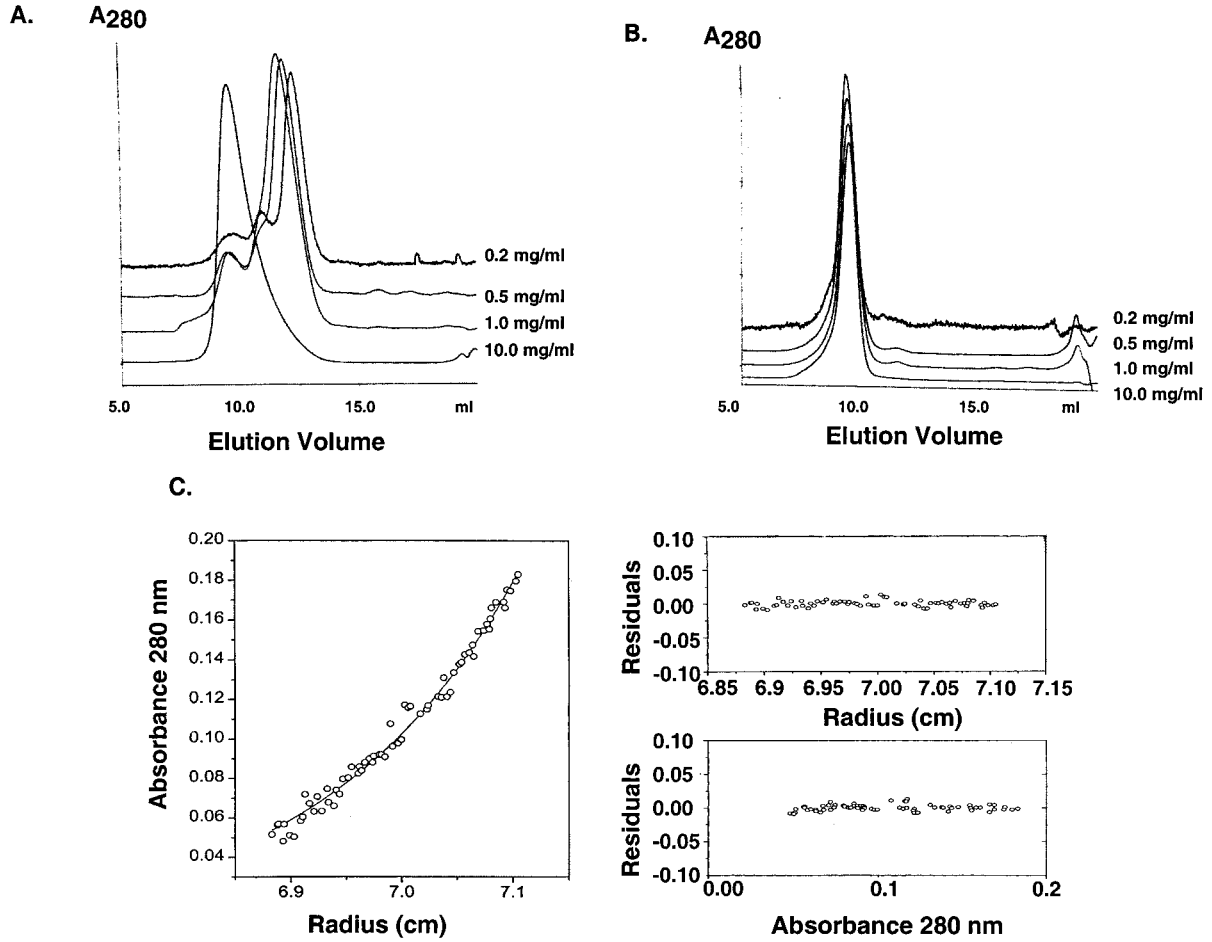

FIGURE 2: Analytical gel filtration of DnaB from *E. coli* (A) and *B. stearothermophilus* (B). DnaB was concentrated to various concentrations as indicated and loaded onto a Superdex S200 gel filtration column. Gel filtration was carried out as described in Experimental Procedures. (C) Analytical gel filtration of *B. stearothermophilus* DnaB. Sedimentation equilibrium analysis of *B. stearothermophilus* DnaB was carried out, and all data were fitted to the equation for a single ideal species. For clarity, the graph shows a subset of all the data acquired at three different protein concentrations (1, 2.5, and 5 μM). Samples were sedimented at 4700 rpm, and protein absorbance was measured at 280 nm. Analysis of the residuals is also shown to verify that the data did not deviate from ideality.

The differences in the oligomerization states of P17 between the *E. coli* and *B. stearothermophilus* proteins either may be explained by the interaction being stronger in the *B. stearothermophilus* P17 fragment or may be due to the fact that the *E. coli* P17 fragment was a proteolytic fragment which further lacked a short peptide at the carboxy-terminus compared to our P17 protein (*30*) and may thus be unable to dimerize. Further experiments must be carried out to clarify this point. Significantly, the crystal structure of the P17 fragment of *E. coli* DnaB has been determined and has been shown to contain dimers in the crystal (*34*), and the dimerization of these domains is suggested to play a part in the C_6 to C_3 transition of the DnaB hexamer. The 6-fold symmetry (C_6) represents hexamers, where the smaller amino terminal domain is monomeric; the intermediate forms represent dimerization of these domains, while molecules with 3-fold symmetry (C_3) are fully dimerized. An NMR structure of the same fragment supported the suggestions drawn from the crystal structure (*35*). Dimerization of *B. stearothermophilus* P17 is also consistent with the symmetry of the *E. coli* DnaB protein seen in electron micrographs (*36*). Since P33 forms a less stable hexamer than the full-length protein, it may be that dimerization of P17 acts to stabilize the hexamer formed by the full-length protein. No interactions were observed between P17 and P33 in low or high salt, suggesting either that the domains are structurally discrete or that the structure of the linking region is essential for the interaction and may not form correctly in the discrete fragments (Figure 3D).

Biochemical Characterization of the B. stearothermophilus DnaB. The kinetics of ATP hydrolysis for *B. stearothermophilus* DnaB was analyzed under steady-state conditions both in the presence and in the absence of ssDNA (81mer oligonucleotide). The enzyme did not obey Michaelis−Menten kinetics under our experimental conditions (Figure 4A). In the absence of DNA, the ATPase activity increased with increasing ATP concentration up to 0.8 mM. Then the activity reached a plateau up to 1.2 mM and started to increase again, reaching a maximum activity at 2.5 mM ATP. Increasing the ATP concentration further resulted in decreasing ATPase activity which was reduced to almost zero at 4.5 mM ATP. Increasing the ATP or $MgCl_2$ concentration further did not recover activity (data not shown). A similar profile was observed in the presence of ssDNA (Figure 4A). However, this time the initial increase in ATPase activity was observed up to 0.25 mM ATP followed by the plateau up to 0.8 mM ATP. Then the activity increased to a maximum at 1.5 mM and started decreasing at higher ATP concentrations, reaching zero at 2.5 mM ATP. Again, increasing the ATP concentration further or adding more

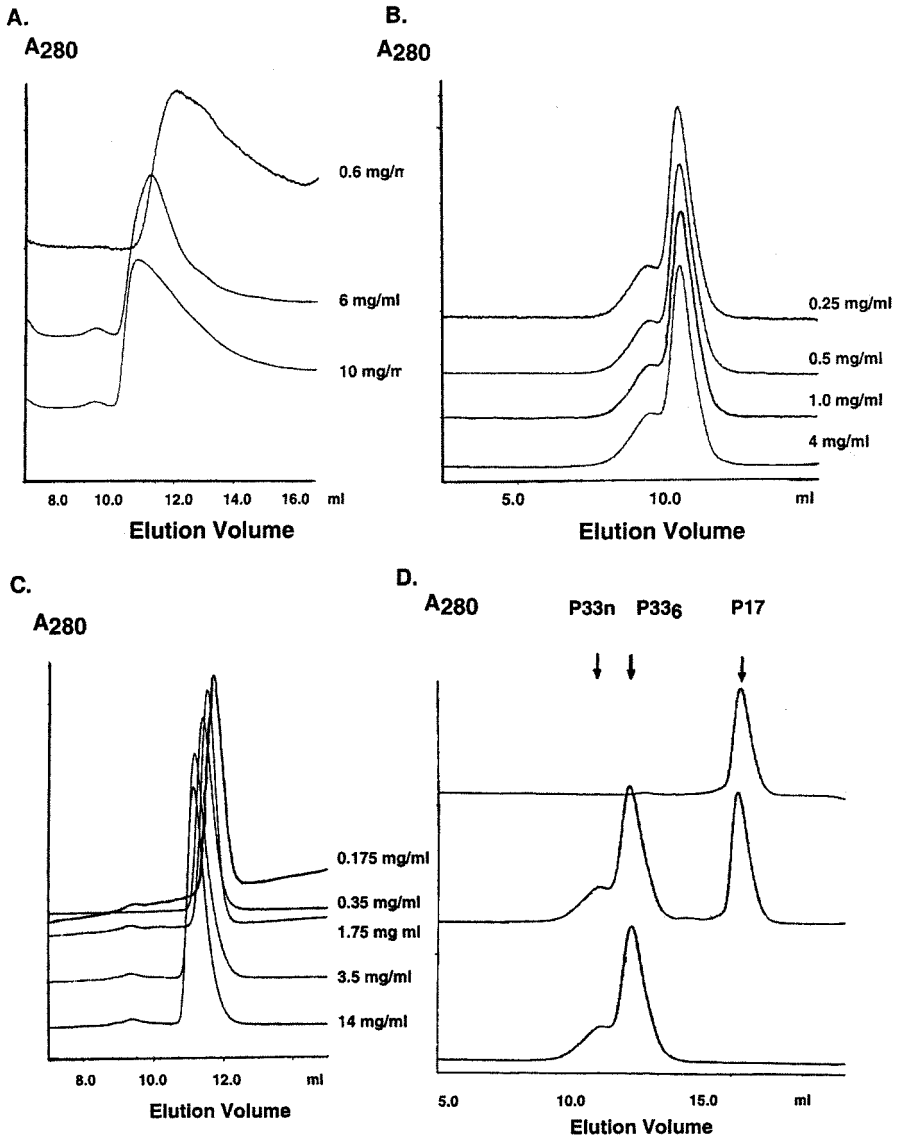

FIGURE 3: Analytical gel filtration of DnaB proteolysis fragments (P33 and P17). P33 was loaded onto a Superdex S200 gel filtration column at various concentrations as indicated. Gel filtrations were carried out at 100 (A) and 500 mM NaCl (B). The same experiment was repeated for P17 using a Superdex S75 gel filtration column (C) and for mixtures of P33 and P17 using a Superdex S200 column (D) at 100 mM NaCl. P33n denotes complexes of P33 formed by aggregation. Similar experiments with P33 and P17 mixtures at 500 mM NaCl also failed to demonstrate interactions between the two polypeptides (data not shown).

$MgCl_2$ did not recover activity (data not shown). Interestingly, the helicase activity of the enzyme also exhibited a similar profile (Figure 4B). It increased with increasing concentration up to 3.75 mM ATP and started decreasing at higher ATP concentrations, reaching zero at 6.25 mM ATP. Once more, increasing the ATP or $MgCl_2$ concentration further did not recover activity (data not shown). In an attempt to explain these peculiar ATPase and helicase activity profiles, one possibility is that, under the conditions of these experiments, DnaB does not exist as a hexamer but that adding more ATP could induce its hexamerization with the consequent observed increase in activity. However, sedimentation equilibrium experiments show that *B. stearothermophilus* DnaB exists as a stable hexamer, in the presence or absence of ATP (or ADPNP) and Mg^{2+}, at a concentration as low as 1 μM (Figure 2C and data not shown). Gel filtration experiments also confirm the stability of the DnaB hexamer, in the absence of ATP and Mg^{2+}, at a concentration as low as 100 nM (data not shown). Furthermore, it is reasonable to assume that for DnaB to exhibit helicase activity it must be in a hexameric form (*29*). It is therefore evident that these peculiar ATPase and helicase activity profiles must be attributed to a stable hexamer and may be the result of cooperativity between the subunits of the hexamer as ATP binds to various active sites in the hexamer rather than hexamer dissociation. This is not a novel idea as nucleotide binding to the hexamer has been shown to be cooperative with three strong and three weak ATP binding sites in the T7 gene 4 helicase (*37*, *38*) and to induce dramatic conformational changes of the hexamer in DnaB (*39*). Although it is difficult to explain these activity profiles, the inactivation of the hexamer at high ATP concentrations is likely to be the result of negative cooperativity, as ATP binds to the three weak sites of the hexamer. In these data, the ATPase activity is expressed as ATP molecules hydrolyzed per second per protein monomer. Because of the negative cooperativity discussed above, not all six monomers of the hexameric ring will be hydrolyzing ATP with the same rate, and therefore, one should be aware of this fact in interpreting the data. Our data also show that the presence of ssDNA

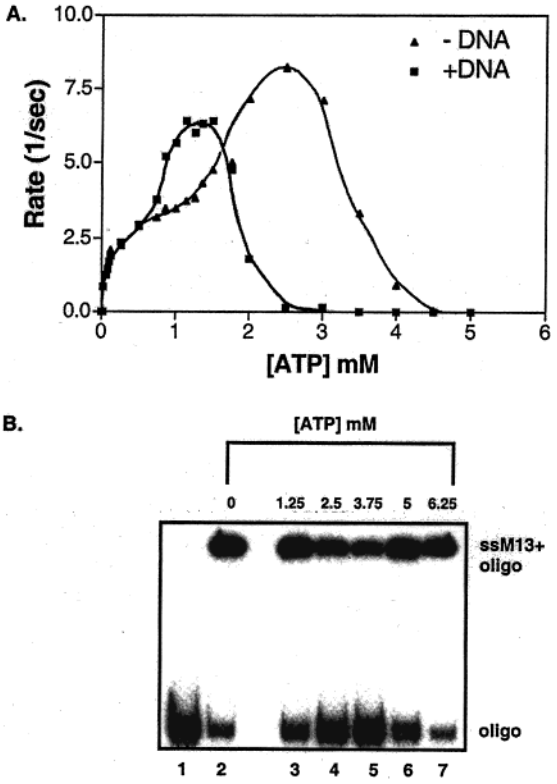

FIGURE 4: ATPase activity profiles of DnaB under steady-state conditions in the presence (■) and absence (▲) of ssDNA cofactor (A). The graphs show the rate of ATPase activity under steady-state conditions vs ATP concentration. The rate of ATPase activity is defined as the number of ATP molecules hydrolyzed per second per DnaB monomer. (B) The effect of increasing ATP concentration on the helicase activity of DnaB. Reactions were carried out at various ATP concentrations as indicated, at 50 °C, for 20 min, as described in Experimental Procedures.

alters the activity profile, shifting the optimal activity with respect to ATP concentration (1.5 mM compared to 2.5 mM in the absence of ssDNA).

P33 possesses all of the conserved ATPase and helicase motifs and exhibits ATPase activity, albeit somewhat reduced compared to that of the intact enzyme. The ATPase activity profile of P33 was very different from that of the full-length DnaB (Figure 5). The activity increased with increasing ATP concentration up to 1 mM and then decreased slightly to a plateau at high concentrations of ATP (up to 6 mM). The ATPase assays were carried out at 24 nM protein and at low salt (50 mM NaCl and 10 mM $MgCl_2$). ATPase activity is expressed as ATP molecules hydrolyzed per second per monomer of protein. Under these conditions, P33 exists as a dimer, and therefore, the ATPase activity profile must be attributed to a dimeric species of P33. Furthermore, it is possible that the P33 dimeric species also exhibits cooperativity with the two monomers hydrolyzing ATP at different rates. As was observed for the DnaB hexamer, ssDNA altered the ATPase activity profile of P33, shifting the optimal activity with respect to ATP concentration (0.5 mM compared to 1 mM ATP in the absence of ssDNA). P33 did not exhibit any detectable helicase activity despite the fact that it contains all of the conserved helicase signature motifs (data not shown). This may be because under our assay conditions, at low salt, P33 cannot form stable hexamers and hexamerization is likely to be a prerequisite for helicase activity. Although at high salt concentrations P33 forms hexamers,

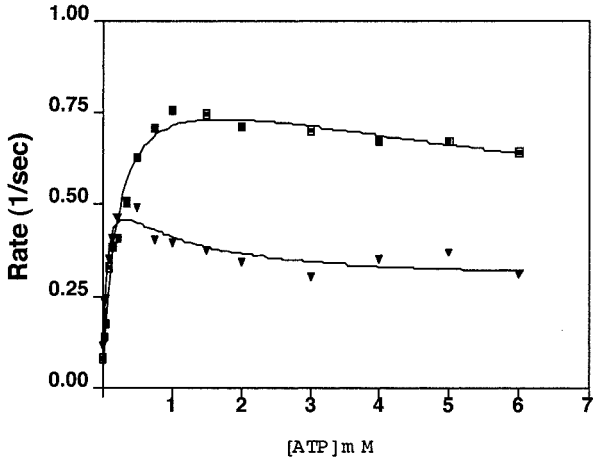

FIGURE 5: ATPase activity profiles of P33 in the presence (▼) and absence (■) of ssDNA. The rate of ATPase activity under steady-state conditions is presented as a function of ATP concentration. The rate of ATPase activity is defined as the number of ATP molecules hydrolyzed per second per P33 monomer. Experimental details are desribed in Experimental Procedures.

it does not bind ATP and therefore exhibits no helicase activity. Alternatively, we cannot rule out the possibility that the N-terminal domain, P17, contributes to the helicase activity of the enzyme. Such a contribution could involve stabilization of the hexamer, enhancement of hexamer binding to DNA, or even direct involvement in the helicase reaction itself.

Isolation of a Stable Complex between DnaB and DnaG. DnaB and DnaG mixtures were subjected to gel filtration, and the resulting fractions were analyzed by SDS−PAGE. DnaG eluted with a molecular mass corresponding to approximately 65 kDa, indicating that the protein is monomeric under these conditions (Figure 6A). This was also supported by sedimentation equilibrium experiments which estimate a molecular mass of 66 kDa, at a DnaG concentration of 15 μM (Figure 6B). This is in very good agreement with the molecular mass of a monomer calculated from the sequence of the protein (67 kDa). In gel filtration experiments, as expected, DnaB eluted with an apparent molecular mass of 300 kDa, indicating a hexameric complex. These data were consistent with sedimentation equilibrium data which also suggested a molecular mass of 300 kDa for DnaB (Figure 2C). In mixtures of the two proteins, a peak was identified which eluted from the gel filtration column earlier than either of the two proteins alone (Figure 6A). SDS−PAGE analysis revealed that this peak contained both proteins, suggesting the formation of a stable complex of DnaB and DnaG (Figure 6A). In equimolar mixtures of the two proteins (in terms of monomers), an additional peak eluted at the position expected for a DnaG monomer. As the ratio of DnaG to DnaB was reduced, the amplitude of this peak also was reduced, and at a ratio of two to three DnaG molecules to one DnaB hexamer, all of the primase was found in the complex, suggesting that the stoichiometry is two or three DnaG molecules per DnaB hexamer (data not shown). The apparent molecular mass of the complex is 470 kDa, estimated from gel filtration experiments. Sedimentation equilibrium experiments estimated a molecular mass of 465 kDa (Figure 6C). The theoretical molecular mass values of DnaB and DnaG complexes, calculated from the protein sequences, are 437 802 Da for a hexamer of DnaB

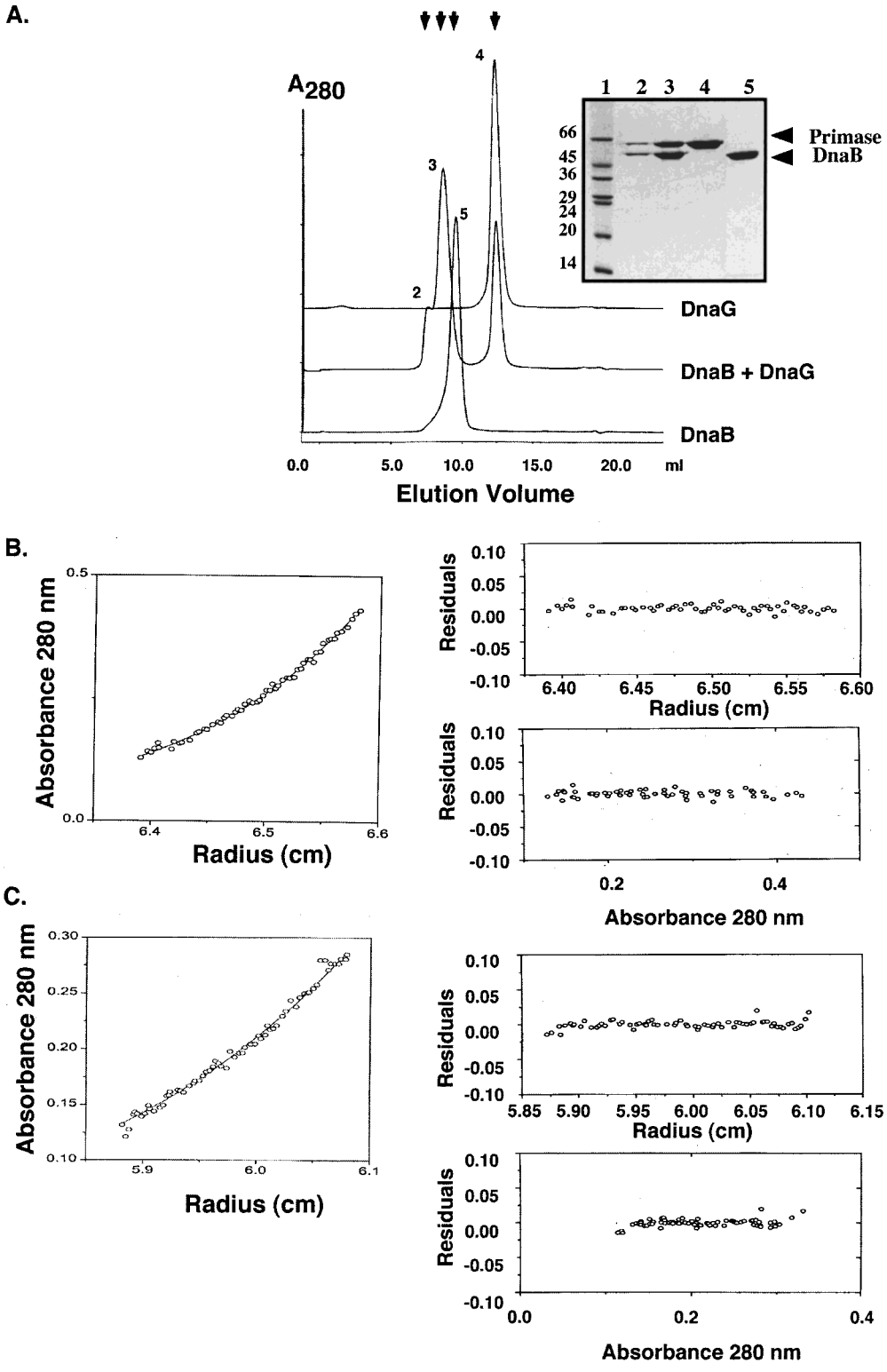

FIGURE 6: (A) Analytical gel filtration of DnaB, DnaG, and the DnaB−DnaG complex. DnaB and DnaG were mixed together at a molar ratio of 1:6 and loaded onto a Superdex S200 gel filtration column. The elution peak of the DnaB−DnaG complex is indicated together with the elution peaks of DnaB and DnaG. Samples from all the elution peaks were analyzed by SDS−PAGE, to verify the presence of the appropriate proteins, as indicated. Lane 1 contained molecular mass markers, and lanes 2 and 3 contained samples from the "shoulder" and the main elution peak of the DnaB−DnaG complex, respectively; lane 4 contained a sample from the DnaG peak, and lane 5 contained a sample from the DnaB peak. Equilibrium sedimentation of DnaG (B) and of the preformed DnaG−DnaB complex (C). All the data were fitted to the equation for a single ideal species. For clarity, the graphs show subsets of all the data acquired at three different protein concentrations (3, 6, and 15 μM for DnaG and 1, 2, and 5 μM for the DnaB−DnaG complex). Samples were sedimented at 11 000 (DnaG) and 3700 rpm (DnaB−DnaG complex). Protein concentrations were measured at 280 nm. Residual plots are also presented to verify that the data did not deviate from ideality.

complexed to two DnaG molecules (six DnaB molecules and two DnaG molecules) and 504 870 Da for a hexamer of DnaB complexed to three DnaG molecules (six DnaB molecules and three DnaG molecules). Both gel filtration

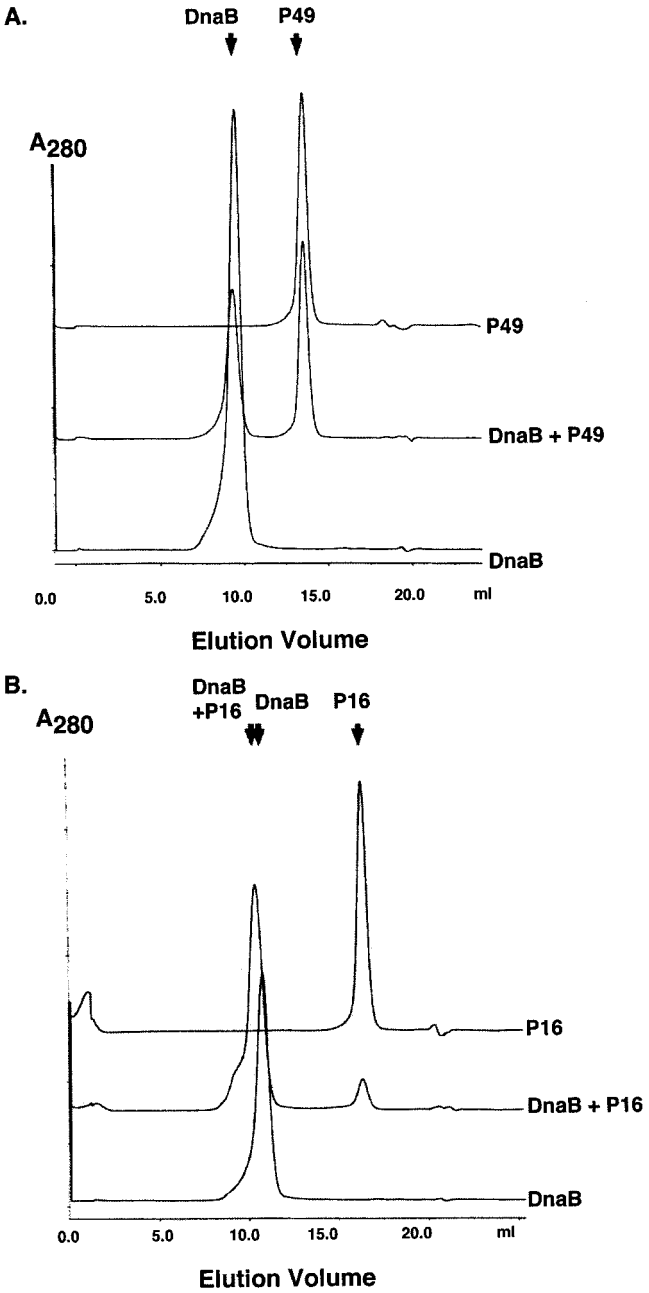

FIGURE 7: Analytical gel filtration of mixtures of DnaB with P49 and P16. Mixtures of DnaB with P49 (A) and P16 (B) were loaded onto a Superdex S200 column. Gel filtration was carried out at low salt (100 mM NaCl) as described in Experimental Procedures. All elution peaks are marked appropriately. For both cases, the same results were obtained when gel filtration was carried out at high salt (500 mM NaCl) (data not shown).

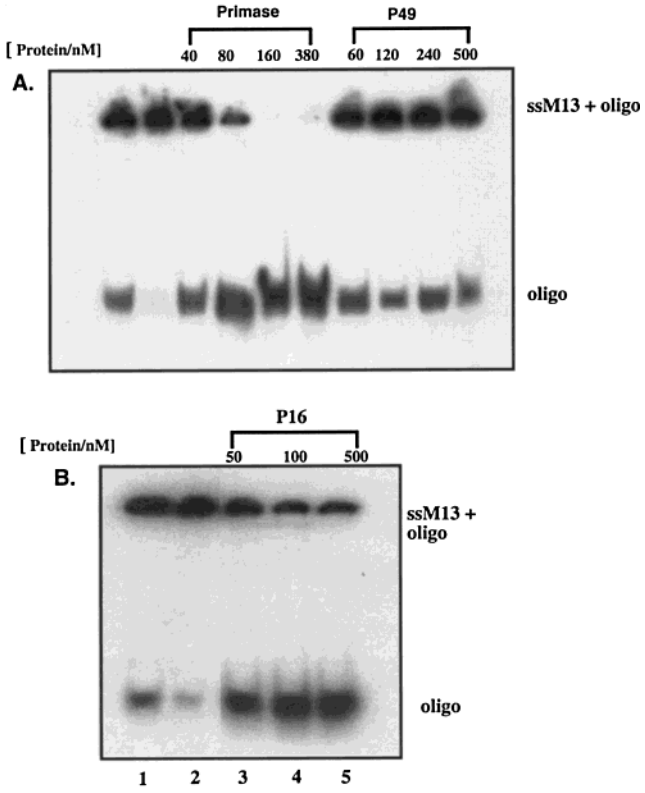

FIGURE 8: Effect of DnaG and P49 on the helicase activity of DnaB (A). Helicase reactions were carried out using 0.1 μM DnaB (referring to monomer), 1 nM DNA substrate, and different concentrations of DnaG (lanes 3−6) and P49 (lanes 7−10). Control reactions with DnaB in the presence (lane 1) and absence (lane 2) of ATP are also shown. The effect of P16 on the helicase activity of DnaB is shown in panel B. Lanes 1 and 2 show DnaB reactions in the presence and absence of ATP, respectively.

and equilibrium sedimentation techniques give estimates for the molecular mass between these two values, making it difficult to identify precisely whether two or three DnaG molecules interact with the DnaB hexamer. Although the gel filtration estimate is likely to be affected by the shape of the DnaB−DnaG complex, the equilibrium sedimentation estimate is independent of the shape of the complex. However, in the latter case, the molecular mass estimate is an average of all species present in the solution. Therefore, even a small degree of dissociation of the complex will result in an underestimate of its molecular mass. Nevertheless, the fact that with both techniques we obtain molecular mass estimates that are consistently higher than the theoretical value for a complex of six DnaB and two DnaG molecules suggests that the stoichiometry of the complex is six DnaB molecules to three DnaG molecules, three DnaG molecules interacting with the DnaB hexamer (calculated mass of 351 kDa).

Mapping Interactions within the DnaB−DnaG Complex. To dissect the interactions between the proteins in the complex, we carried out gel filtration experiments with different fragments of DnaG (P49 and P16) to determine which region of the primase interacts with DnaB (Figure 7). These results show that P49 is not capable of forming a complex with DnaB (Figure 7A). In contrast, P16 forms a tight complex that is stable during gel filtration (Figure 7B). This complex elutes with an apparent molecular mass of 350 kDa, suggesting three molecules of P16 interacting with the DnaB hexamer. Gel filtration titration experiments of P16 with DnaB and sedimentation equilibrium experiments, similar to those carried out with the intact DnaG, were consistent with two or three P16 molecules interacting with one DnaB hexamer (data not shown).

In *E. coli* primase, the N-terminal 49 kDa domain (P49) is responsible for priming while the C-terminal 16 kDa domain (P16) is responsible for interacting with DnaB (*28*). We utilized helicase and ATPase assays to study biochemically the interaction between the *B. stearothermophilus* DnaG and DnaB proteins (Figure 8). DnaG has no intrinsic helicase activity, but when added to a helicase assay containing DnaB, it stimulates the helicase activity of DnaB. P49 is unable to

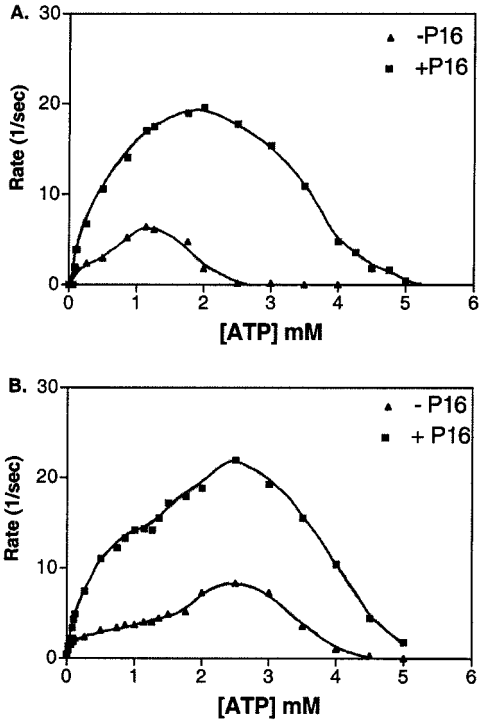

FIGURE 9: Effect of P16 on the ATPase activity of DnaB in the presence (A) and absence (B) of ssDNA. ATPase reactions were carried out at various ATP concentrations as described in Experimental Procedures, in the presence of 160 μM P16. The results are presented in a graph showing the rate of ATPase activity under steady-state conditions vs the concentration of ATP. The rate of ATPase activity is defined as the number of ATP molecules hydrolyzed per second per DnaB monomer.

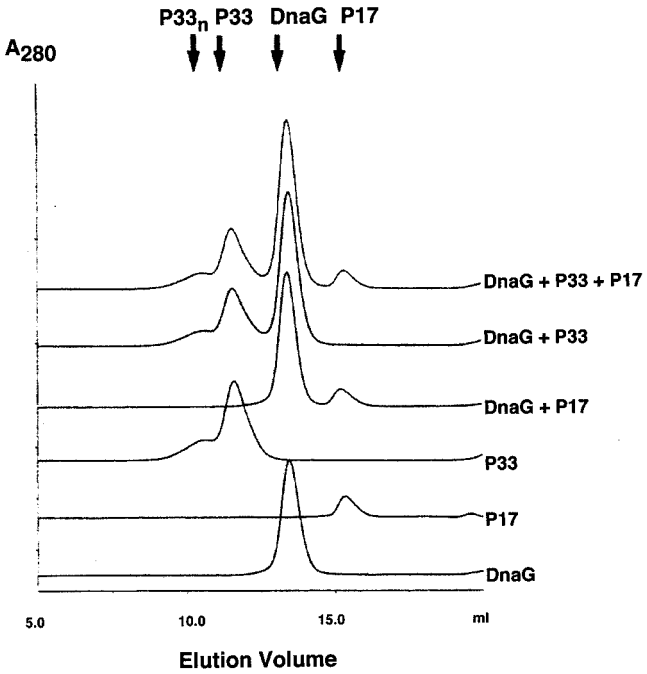

FIGURE 10: Analytical gel filtration of mixtures of DnaB fragments (P33 and P17) with primase. Mixtures of DnaB with P33 and P17 were loaded onto a Superdex S200 gel filtration column, and gel filtration was carried out as described in Experimental Procedures at low salt (100 mM NaCl). P33n denotes complexes of P33 formed by aggregation. The elution peaks of all proteins are indicated appropriately. No association of the two fragments with DnaG could be detected. The same result was obtained when the experiment was repeated at high salt (500 mM NaCl) (data not shown).

induce this stimulation even at higher concentrations (Figure 8A). By contrast, P16 stimulates the helicase activity of DnaB (Figure 8B). These data confirm biochemically the suggestion that it is the C-terminal domain of primase that mediates the interaction with DnaB (*28*). However, the molecular mechanism of this stimulation is unclear. In the presence of P16, there is a significant stimulation of the ATPase activity of DnaB (Figure 9) which may also explain the associated stimulation of its helicase activity, if ATPase activity is rate-limiting in the helicase reaction (Figure 8B). This stimulation is evident in the presence or absence of the ssDNA cofactor. Full-length DnaG gives similar results, but no stimulation of the ATPase activity is observed in the presence of P49 (data not shown). These data suggest that binding of primase to DnaB, via the P16 domain, modulates the conformation of the hexamer, thus affecting its activity.

The contribution of DnaB to the formation of the complex is more complex. Gel filtration experiments show that although the C-terminal P33 fragment of DnaB is able to form stable hexamers at high salt (Figure 3B), it is not able to form a complex with DnaG at either low or high salt (Figure 10). Even the addition of the N-terminal P17 fragment of DnaB does not promote complex formation. Although the P33 and P17 fragments do not form a stable complex between themselves (Figure 3D), they do have distinct biochemical properties which suggest that they are not simply misfolded, but that their interaction requires the linker domain that joins them in the intact protein. Consequently, we conclude that the primase binding site is situated across the domain interface of DnaB, with contributions from both the N- and C-terminal domains, and that the linker region is required to maintain this surface in a form that is able to interact with DnaG. However, we cannot rule out the possibility that the linker region is misfolded locally and thus unable to mediate the helicase primase interaction.

CONCLUSIONS

Although it is widely assumed that DnaB and DnaG must form a complex at the replication fork, a lack of direct evidence for such a complex has led to the proposal that the complex is transient. Biochemical data for the *E. coli* enzymes have provided evidence for this proposal. However, this may not be the general case. For example, in bacteriophage T7, the two enzyme activities are encoded by the same polypeptide (gene 4 protein), thereby ensuring a physical coupling of activity. However, in this system there is a complication because the two proteins are encoded by the same gene but begin at different in-frame start points, resulting in a mixture of proteins, known as 4A and 4B. The 4A protein has both helicase and primase activities, but 4B lacks the primase activity due to deletion of 64 amino acids at the N-terminus. In vivo, the active complex appears to be a mixture of the two proteins. It is therefore difficult to estimate accurately the stoichiometry of the active complex. However, in bacteriophage T4, one primase (gp61) was shown to bind six helicase (gp41) subunits and form a stable primase−helicase complex during the assembly of the T4-coded primosome at the replication fork (*40*).

In *Bacillus*, it is clear that there are homologues of the *E. coli* dnaB and dnaG genes (*17*, *18*). In this study, we show that, unlike the *E. coli* proteins, the *B. stearothermophilus* enzymes form a tight complex that we have been able to

isolate by gel filtration. Using a combination of limited proteolysis, gel filtration, and ultracentrifugation techniques, in conjuction with standard biochemical assays (ATPase and helicase assays), we have dissected the contributions of both proteins to the formation of this complex. We showed that it is the 16 kDa C-terminal domain of DnaG that interacts with the interface of both the N- and C-terminal domains of DnaB. This interaction involves two or three primase molecules per helicase hexamer. The result of this interaction is the stimulation of the ATPase and helicase activities of the helicase. Finally, we show that the 33 kDa C-terminal domain of DnaB is capable of forming hexamers and exhibits ATPase activity, albeit somewhat reduced compared to that of intact DnaB.

ACKNOWLEDGMENT

We express our gratitude to Val Cooper for synthesis of the oligonucleotides, Ken Marians for the gift of *E. coli* DnaB, Tony Willis for protein sequencing, Amarjit Bhomra for DNA sequencing, and Jennifer Byrne for technical assistance. Atomic absorption spectroscopy was carried out by J. Kench.

REFERENCES

1. Kornberg, A., and Baker, T. A. (1992) *DNA Replication*, 2nd ed., W. H. Freeman and Co., New York.
2. Tougu, K., and Marians, K. J. (1996) *J. Biol. Chem. 271*, 21398−21405.
3. Zechner, E. L., Wu, C. A., and Marians, K. J. (1992) *J. Biol. Chem. 267*, 4054−4063.
4. Lu, Y., Pillarisetty, V. A., Ratnakar, V. A. L., Mohanty, B. K., and Bastia, D. (1996) *Proc. Natl. Acad. Sci. U.S.A. 93*, 12902−12907.
5. Wu, C. A., Zechner, E. L., and Marians, K. J. (1992) *J. Biol. Chem. 267*, 4030−4044.
6. Bernstein, J. A., and Richardson, C. C. (1989) *J. Biol. Chem. 264*, 13066−13073.
7. LeBowitz, J. H., and McMacken, R. (1986) *J. Biol. Chem. 261*, 4738−4748.
8. Reha-Krantz, L. J., and Hurwitz, J. (1978) *J. Biol. Chem. 253*, 4043−4050.
9. Bujalowski, W., Klonowska, M. M., and Jezewska, M. J. (1994) *J. Biol. Chem. 269*, 31350−31358.
10. Marszalek, J., and Kaguni, J. M. (1994) *J. Biol. Chem. 269*, 4883−4890.
11. Wickner, S., and Hurwitz, J. (1975) *Proc. Natl. Acad. Sci. U.S.A. 72*, 921−925.
12. Kim, S., Dallman, H. G., McHenry, C. S., and Marians, K. J. (1996) *Cell 6*, 643−650.
13. Marians, K. J. (1992) Prokaryotic DNA replication, *Annu. Rev. Biochem. 61*, 673−719.
14. Sakamoto, Y., Nakai, S., Moriya, S., Yoshikawa, H., and Ogasawara, N. (1995) *Microbiology (Reading, U.K.) 141*, 641−644.
15. Wang, L., Price, C. W., and Doi, R. H. (1985) *J. Biol. Chem. 260*, 3368−3372.
16. Bruand, C., Ehrlich, S. D., and Janniere, L. (1995) *EMBO J. 14*, 2642−2650.
17. Bird, L. E., and Wigley, D. B. (1999) *Biochim. Biophys. Acta 1444*, 424−428.
18. Pan, H., Bird, L. E., and Wigley, D. B. (1999) *Biochim. Biophys. Acta 1444*, 429−433.
19. Casabadan, M. C. (1980) *J. Mol. Biol. 138*, 179−207.
20. Bullock, W. O., Fernadez, J. M., and Short, J. M. (1987) *BioTechniques 5*, 376−379.
21. Wood, W. B. (1966) *J. Mol. Biol. 16*, 118−133.
22. Sambrook, J., Fritsch, E. F., and Maniatis, T. (1989) *Molecular Cloning: A Laboratory Manual*, 2nd ed., Cold Spring Harbor Laboratory Press, Cold Spring Harbor, NY.
23. Laemmli, U. K. (1970) *Nature 277*, 680−685.
24. Pullman, M. E., Penefsky, A., Datta, A., and Racker, E. (1960) *J. Biol. Chem. 235*, 3322−3329.
25. Soultanas, P., Dillingham, M. S., Papadopoulos, F., Phillips, S. E. V., Thomas, C. D., and Wigley, D. B. (1999) *Nucleic Acids Res. 27*, 1421−1428.
26. Mendelman, L. V., Beauchamp, B. B., and Richardson, C. C. (1994) *EMBO J. 13*, 3909−3916.
27. Stamford, N. P. J., Lilley, P. E., and Dixon, N. E. (1992) *Biochim. Biophys. Acta 1132*, 17−25.
28. Tougu, K., Peng, H., and Marians, K. J. (1994) *J. Biol. Chem. 269*, 4675−4682.
29. Lohman, T. M., and Bjornson, K. P. (1996) *Annu. Rev. Biochem. 65*, 169−214.
30. Biswas, S. B., Chen, P.-H., and Biswas, E. E. (1994) *Biochemistry 33*, 11307−11314.
31. Nakayama, N., Arai, N., Kaziro, Y., and Arai, K. (1984) *J. Biol. Chem. 259*, 88−96.
32. Bird, L. E., Håkannsson, K., Pan, H., and Wigley, D. B. (1997) *Nucleic Acids Res. 25*, 2020−2026.
33. Bird, L. E., Subramanya, H. S., and Wigley, D. B. (1998) *Curr. Opin. Struct. Biol. 8*, 14−18.
34. Fas, D., Bogden, C. E., and Berger, J. M. (1999) *Structure 7*, 691−698.
35. Weigelt, J., Brown, S. E., Miles, C. S., Dixon, N. E., and Otting, G. (1999) *Structure 7*, 681−690.
36. Egelman, E. D. (1996) *Structure 4*, 759−762.
37. Hingorani, M. M., and Patel, S. S. (1996) *Biochemistry 35*, 2218−2228.
38. Patel, S. S., and Hingorani, W. W. (1995) *Biophys. J. 68*, 186s−190s.
39. Jezewska, M. J., and Bujalowski, W. (1996) *J. Biol. Chem. 271*, 4261−4265.
40. Jing, D. D., Dong, F., Latham, G. L., and von Hippel, P. H. (1999) *J. Biol. Chem. 274*, 27287−27298.

BI9918801